Impact of electric charge and motion of water drops on the inception field strength of partial discharges

Jens-Michael Löwe* and Volker Hinrichsen
High-Voltage Laboratories, Technical University of Darmstadt, Darmstadt, Germany

Ilia V. Roisman and Cameron Tropea
Institute of Fluid Mechanics and Aerodynamics, Technical University of Darmstadt, Darmstadt, Germany

(Received 3 August 2020; accepted 19 November 2020; published 8 December 2020)

Strong electric fields may deform drops and induce their oscillation or motion on the substrate. Moreover, they can initiate partial discharges (PDs) because of the enhancement of the electric field in the vicinity of the three-phase contact lines. The partial discharges affect the drop spreading which can result in unusual drop shapes. In addition, the partial discharges can also deteriorate the surface properties of the substrate, e.g., of high-voltage composite insulators. In this study the occurrence of partial discharges due to stationary or oscillating sessile drops under the influence of an alternating electric field is investigated using a generic insulator model under well-defined conditions. Drops of a yield stress fluid (a gelatin-water mixture) are used to determine the PD inception field strength for stationary drop shapes. The influence of the volume as well as the distance between the individual drops for two drop configurations on the PD inception threshold is determined. The inception field strength of the partial discharges is measured for various drop volumes, drop charges, as well as for different resonance modes of drop oscillations. Besides the electrical measurement, the location of the partial discharges is optically determined by a UV camera. The detailed knowledge of the influencing factors of the partial discharges improves the understanding of the drop behavior under the impact of strong electric fields.

DOI: 10.1103/PhysRevE.102.063101

I. INTRODUCTION

Liquid drops, especially water drops, are highly affected by electric fields [1–4]. The electric field can lead to a deformation, oscillation, or movement of the drop depending on the geometry, liquid, or the electric field. This influence is used in several technical applications like electrowetting [5–7], atomizing of liquids [8,9], and electrospinning [10,11]. The interaction of a drop and the electric field is a complex phenomenon of mutual interaction. The shape of the drop is determined by the electric field but simultaneously the resulting shape can affect the field distribution around the drop. Hence, the interaction can be used to actively manipulate liquids with respect to their shape, an example being optical lenses [12–14].

In contrast, the interaction of liquids and electric fields may also be of detrimental nature, as occurs with high-voltage composite insulators. Insulators are specially designed to withstand different environmental and electrical stresses. The aim is to reduce creeping currents on the surface as well as to prevent flashovers to guarantee safe and reliable operation. Typically, the surface of high-voltage composite insulators is made hydrophobic by using a silicone rubber, which prevents the formation of conductive liquid layers. Thus, instead of a liquid layer, only single sessile drops are formed on the hydrophobic surface.

The field distribution is mainly influenced by the properties of the water, namely, the conductivity and the permittivity, and the frequency of the electric field [15,16]. The charge relaxation time of water is defined by $\tau_e = \varepsilon/\sigma_{el}$, where ε is the permittivity and σ_{el} is the electrical conductivity [17]. Even for deionized water $\tau_e \ll 1$ so water can be assumed as a perfect conductor. As a result the electric field inside the drop completely vanishes. However, this is only valid for $\tau_e \ll 1/f$, where f is the frequency of the electric field. For electric fields with higher frequencies ($\tau_e \gg 1/f$) the water can be assumed to be a leaky dielectric. In this case the high permittivity of water ($\varepsilon_r \approx 80$) leads to an electric field displacement inside the drop and an enhancement of the electric field in the air close to the three-phase contact line due to its low permittivity $\varepsilon_{r,air} = 1$. Both conducting and dielectrics generate high electric field strength directly at the three-phase contact line, resulting in the generation of electrical partial discharges at the three-phase contact line. These electrical critical points are caused by the different electrical properties of the involved materials, namely, silicone rubber, water, and air. The partial discharges generate locally higher temperatures and UV light, which can deteriorate the surface properties and result in an accelerated aging process of the insulator.

The generation of partial discharges is affected by drop motion, drop charge, or surface contamination. Several studies were performed in the past to identify and investigate these influencing factors, including the behavior of single sessile drops and the related partial discharge generation [18–20]. In addition, the influence of the insulator geometry and the material properties were investigated by accelerated aging tests [21–23]. Many investigations have been performed with a focus on electrowetting [6,24,25]. However, most of these

*jens-michael.loewe@tu-darmstadt.de

investigations used a classical electrowetting setup, where the drop is always in contact with one of the electrodes and essentially extends the electrode. For these setups the field enhancement at the three-phase contact line was theoretically investigated and the occurrence of partial discharges was optically recorded [26]. Furthermore, the classical electrowetting setup was analyzed in detail with respect to charge accumulation and the mechanisms at the three-phase contact line [27]. The role of charge accumulation at the contact line for a drop in direct contact with an electrode was also investigated in detail [28]. Recently, electric charges were observed to also influence the motion of drops under the influence of electric fields [29], thus possibly influencing the generation of partial discharges. However, the mechanisms of partial discharge generation of a drop without contact to one of the electrodes, as well as the subsequent influence on the aging process of the substrate, is not yet completely understood. Consequently, a reliable predictive model of this phenomenon is not yet available.

In the present experimental study the field strength for the inception of electric partial discharges for moving and stationary drops is investigated. Stationary drops of yield stress fluids are investigated to reduce the complexity of the mechanism and to generate data for simplified models. A mixture of water and gelatin is used to generate stationary drops with electrical properties similar to water. The influence of the drop volume as well as the wetting properties on the inception field strength for partial discharge are investigated. In addition to the single drops, the interaction of nearby drops with respect to the drop-drop distance and their volume is determined. The results of the fixed drops should improve the general understanding of the partial discharge generation for a drop-like geometry. Furthermore, the partial discharge inception of moving, charged, and uncharged drops is investigated to determine the impact of the drop movement, the resonance frequency, as well as the electric charge of a drop. This experimental investigation should help to improve the understanding of the behavior of water drops under the influence of electric fields and of the aging process of composite insulators.

II. EXPERIMENTAL SETUP

The partial discharge inception of sessile drops is investigated using a generic insulator model. The drop is placed on the surface of the cuboid specimen made out of silicone rubber (Wacker Powersil 600, $\theta_a \approx 116^\circ \pm 4^\circ$, $\theta_r \approx 65^\circ \pm 2^\circ$) or epoxy (Ciba Araldit F, Ciba Hardener HY 905 and SILBOND W 12 EST with a weight portion of 16.4%, 16.4%, and 65.5%, respectively; $\theta_a \approx 89^\circ \pm 4^\circ$, $\theta_r \approx 20^\circ \pm 3^\circ$). Two electrodes are embedded into the basis material to generate a tangentially aligned electric field on the surface of the specimen. A tangentially aligned electric field was chosen because of the higher impact on the drop motion [29,30] and as it represents typical electric stress on insulator surfaces. Figure 1 shows the geometry of the specimen. An alternating voltage with a value of up to $\hat{U} = 20$ kV is supplied to one of the electrodes, while the other electrode is grounded. A signal generator (GW Instek SFG-2104) is used to generate a variable sinusoidal signal with a frequency between 10 and 100 Hz, which supplies a self-constructed amplifier. The high voltage is generated by

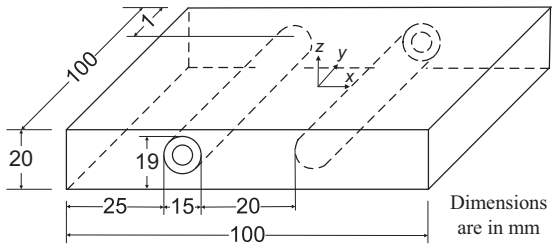

FIG. 1. Schematic of the specimen, reprinted figure with permission from [29].

a high-voltage transformer (type MWB TEO 100/10) using the amplified sinusoidal signal. The voltage level as well as the partial discharge inception is measured using a commercially available measurement system (Omicron MPD 600). The electrical circuit is designed according to the International Electrotechnical Commission (IEC) 60270 standard to guarantee an accurate measurement of the inception voltage for partial discharges. The setup was calibrated using a defined charge of $Q_{PD} = 1$ pC (Omicron CAL 542) as required, and the threshold for the partial discharge detection was set to $Q_{PD} = 5$ pC.

During the experiment the partial discharge activity is recorded using the MPD software from Omicron to record the charge of each partial discharge impulse and the corresponding voltage level. Afterwards the data are analyzed using an in-house MATLAB code to accurately determine the inception voltage for the threshold charge of $Q_{PD} = 5$ pC. Based on the inception voltage, the inception field strength is determined using an electric field simulation of the experimental setup (performed with Comsol Multiphysics) shown in Fig. 1. The resulting electric field strength is the corresponding electric field strength in the absence of a drop directly at the center of the specimen surface (see origin of coordinate system in Fig. 1) and is used to specify the inception field strength.

The voltage divider used for the measurement of the voltage level was calibrated using a reference prior to the measurement. To reduce the impact of external influences, the experimental setup is placed inside a shielded and grounded chamber. Hence, the background noise for the partial discharge measurement is only $Q_{PD} \approx 300$ fC. The partial discharge inception field strength for the overall test setup without a drop is $\hat{E}_{in} \approx 9.2$ kV/cm and is not reached during the measurements.

In addition to the electrical measurement of partial discharges, the drop is observed by a UV camera (PCO pco.edge 4.2 bi UV) with a UV sensitive lens (UV-Nikkor 105 mm). The UV camera is used to locate the origin of the partial discharges with up to 40 fps. Images are captured in side view or in top view to correlate the electrical data to the image data as shown in Fig. 2. To ensure a high quality of the UV images all light sources are switched off and external light is prevented from entering the chamber by curtains.

III. DROP GENERATION

A single drop of given volume is generated by an automated syringe. The position at the substrate center is

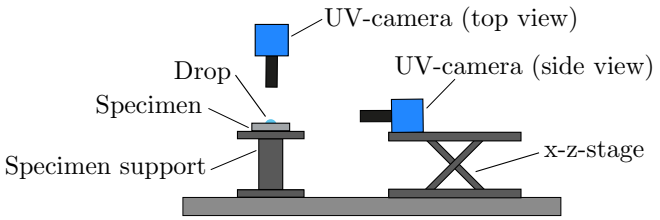

FIG. 2. Schematic of the experimental setup. The UV camera is used either in top or in side view.

controlled by a positioning system. High-purity water (Millipore Milli-Q type I) with an electrical conductivity of $\sigma_{el} = 5.5 \times 10^{-6}$ S/m (at 25°C) is used for water drops. The charge relaxation time of water yields $\tau_e = \varepsilon/\sigma_{el} = 1.30 \times 10^{-4}$ s, so that water drops can be assumed to be a perfect conductor for the given frequency range ($\tau_e \ll 1/f_{max} = 1 \times 10^{-2}$ s). Prior to the drop deposition, the surface of the substrate is cleaned using wet antistatic wipes to reduce the surface charges [31]. Each experiment is performed with a fresh drop and a cleaned surface to minimize the effect of accumulated charges. With water drops, the substrate is used several times and is cleaned after each experimental run. In contrast, for gelatin drops each experiment is performed with a new substrate due to the time-consuming production method, which is subsequently described. To minimize the effect of surface aging the substrate was visually inspected prior to each experiment and the static contact angle was determined for each experiment to detect a change of the wettability of the substrate, which are common methods in high-voltage engineering to characterize the aging of a substrate (see, e.g., IEC technical specification 62073). If any changes were observed the substrate was replaced.

A. Charging of a water drop

The charging of the water drop is performed with an automated syringe and a drop charger, similar to [29,32]. A schematic of the drop charger is shown in Fig. 3. Two parallel disk electrodes are used to generate an electric field. Water is forced by an automated syringe to flow through the needle, which is connected to the high-voltage electrode. The flow rate is kept constant during the drop generation. As soon as the drop detaches from the needle the drop falls through the hole in the bottom electrode and is charged due to charge separation. The drop charger is placed directly above the specimen without touching the surface to prevent the generation of surface charges. The position of the drop charger ensures that

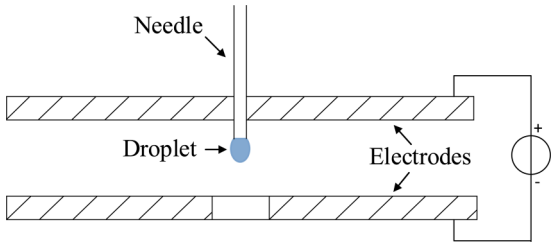

FIG. 3. Schematic of the drop charger, reprinted with permission from [29].

the drop is always placed in the center of the specimen. The actual charge on the drop is proportional to the voltage applied to the drop charger and depends on the drop volume. For an accurate and repeatable charge generation the complete setup was calibrated prior to the measurements as described in [29]. Thus, the charge on the drop can be controlled very accurately with an uncertainty of $\Delta Q = 5.5$ pC. The drop charger is also used to generate uncharged drops. In this case both electrodes of the drop charger are grounded. The resulting drop has a charge lower than $Q = 5.5$ pC.

Generally, the charge of a drop is limited, depending on the drop volume and surface tension [3]. The maximum charge Q_{max} of a drop is given by the Rayleigh limit [3]

$$Q_{max} = \sqrt{48\pi\varepsilon_0\gamma V}, \tag{1}$$

where ε_0 is the vacuum permittivity, γ is the surface tension, and V the drop volume. Note that drops which contain a charge close to Q_{max} might already be deformed. Hence, the drop charge in this study was limited to values without visible deformation.

B. Preparation and characterization of gelatin drops

The occurrence of partial discharges is mainly influenced by the involved materials and their properties, namely, their conductivity and permittivity. Hence, the generation of stationary drops has to be performed with caution, to be able to reproduce the properties of water drops as accurately as possible. In this study a mixture of water and gelatin is used to produce a stationary drop with nearly the same electrical properties. High-purity water is mixed with gelatin (Sigma Aldrich G9391, Bloom number ≈225) with a weight ratio of 25:1 (25 g of water and 1 g of dry gelatin powder), respectively. The mixture is heated to a temperature of $\vartheta \approx 70°$ C and simultaneously stirred for at least 5 min to fully dissolve the gelatin. Subsequently, drops are generated using the automated syringe on the surface of the specimen. Then, the specimen with the sessile drop is placed inside a refrigerator at a temperature of $\vartheta = 9°$ C for approximately 1 h to solidify the drop. Note that the longer the time of storage, the more likely is an evaporation of the drop. Hence, the storage time should be as short as possible. The electrical conductivity of the water-gelatin mixture was measured and is in the same order of magnitude as the electric conductivity of water (10^{-5} S/m). Figure 4 shows the measurement of the relative permittivity of the water-gelatin mixture for different temperatures in the solid state for frequencies between $f = 0.1$ and $f = 1$ MHz. As shown in the figure, water has a constant relative permittivity of $\varepsilon_r \approx 80$ for high frequencies ($f > 10^5$ Hz). A decreasing frequency leads to electrode polarization (Maxwell-Wagner-Sillars phenomenon) [33], which influences the outcome of the measurement and leads to extremely large and technical nonrelevant values of the permittivity. The electrode polarization depends on the electrode configuration and will always appear during the measurement. For the given measurement shown in Fig. 4 the electrode polarization (increase of the permittivity) is only observable for the water-gelatin mixture. For water the increase is observable only at lower frequencies ($f \approx 10^4$ Hz). Due to the Maxwell-Wagner-Sillars phenomenon it is widely accepted to assume a

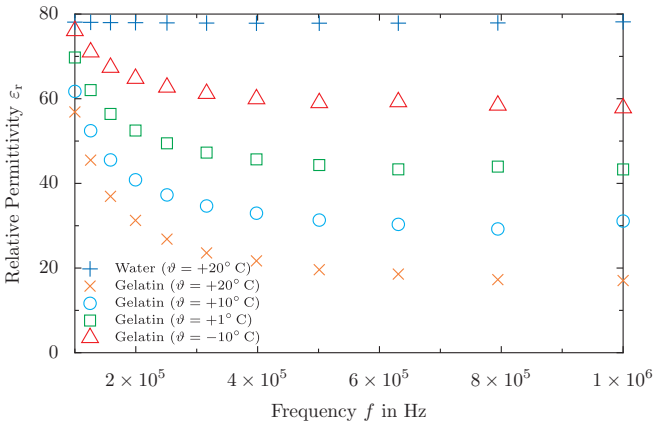

FIG. 4. Frequency-dependent relative permittivity of water and gelatin at different temperatures ϑ.

constant relative permittivity of water also for low frequencies ($f < 1$ GHz) [33], which depends on the temperature [34] and is measured at higher frequencies (like $f = 10^6$ Hz in this case). In comparison to water, the relative permittivity of the water-gelatin mixture is lower.

Since the permittivity of water is assumed to be constant even for low frequencies (like $f = 50$ Hz), it is possible to assume that the gelatin-water mixture has also a constant permittivity, which can be determined at high frequencies ($f = 10^6$ Hz). Figure 4 shows a strong dependence of the relative permittivity on the temperature. An increasing temperature leads to a decrease of the relative permittivity. Hence, the temperature of the gelatin drop should be as low as possible to recreate the physical situation.

Calculating the charge relaxation time using the measured electrical conductivity and the permittivity leads to $\tau_e = \varepsilon/\sigma_{el} \approx 10^{-5}$ s for a permittivity $\varepsilon_r = 20$ and assuming the same electrical conductivity as pure water. Due to the fact that $\tau_e \ll 10^{-2}$ s, also the water-gelatin drops can be assumed to be a perfect conductor for the given frequencies of the electric field. As a consequence, the electric field inside the water-gelatin drop vanishes, similar to pure water. Thus, the water-gelatin mixture perfectly reproduced the electrical behavior of a liquid water drop for the investigated frequencies of the electric field.

Due to the fact that the inflexible drops evaporate at room temperature the experiment has to be performed directly after the specimen is taken out of the refrigerator. To ensure well-defined boundary conditions the temperature of the drop is randomly checked using a handheld thermal camera. However, the volume of the gelatin drops was chosen between $V = 100$ and $V = 300$ μl, for which the effect of evaporation is negligibly small.

IV. COMPARISON OF GENERAL BEHAVIOR OF WATER AND GELATIN DROPS

Gelatin and water drops are assumed to have a similar behavior with respect to the occurrence of partial discharges at the three-phase contact line. The visual investigation of partial discharges was already performed by, e.g., Vallet *et al.* [26] for the classical electrowetting setup with a drop in direct contact

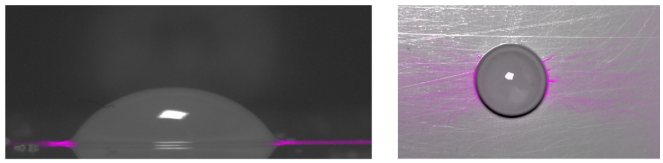

(a) (b)

FIG. 5. Exemplary images of gelatin drops: (a) $V \approx 65$ μl and (b) $V \approx 130$ μl with superimposed image of UV camera to visualize the partial discharges (colored in magenta) in (a) side view for $\hat{E} = 12.48$ kV/cm and (b) top view for $\hat{E} = 10.27$ kV/cm.

with one of the electrodes. The partial discharges are generated directly at the three-phase contact line. In the present experimental setup the drops are not in direct contact with one of the electrodes. Hence, the influence of the different experimental setup can be deduced. In addition, a comparison based on the images taken from the UV camera is shown in Figs. 5 and 6. The drops are shown in side view and in top view. The image of the UV camera capturing the partial discharges is superimposed onto a regular image of the drop. Note that the intensity of the partial discharges in the pictures is individually adjusted to increase the visibility; therefore, the strength of the partial discharges cannot be directly compared between the images. Nevertheless, the intensity of the partial discharges in each individual image corresponds to the intensity of the color. Figure 5 shows the partial discharges for a gelatin drop. The shape of the drop is not affected by the electric field and is given by a capped sphere. The partial discharges occur at the three-phase contact line, but only in regions which are oriented towards the electrodes (on the right and left side of the drop). The remaining part of the three-phase contact line does not exhibit any partial discharges. This behavior significantly differs from the results of Vallet *et al.* [26], in which partial discharges were observed at all positions around the drop perimeter. This results from the orientation of the electric field, which is tangentially aligned to the substrate and, therefore, is not symmetrically distributed around the drop.

In contrast to the gelatin drop, the water drop is clearly deformed by the electric field, even for a lower electric field strength. The shape of the drop is very irregular and not a capped sphere anymore. The side view [Fig. 6(a)] illustrates the origin of the partial discharges at the three-phase contact line, while the top view [Fig. 6(b)] shows a different pattern of the partial discharges in comparison to the gelatin

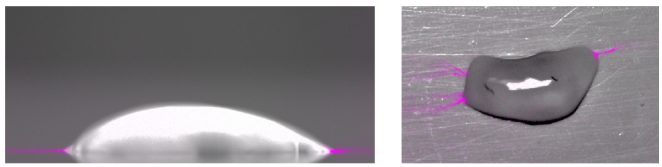

(a) (b)

FIG. 6. Exemplary images of water drops ($V = 20$ μl) with superimposed image of UV camera to visualize the partial discharges (colored in magenta) in (a) side view for $\hat{E} = 9.02$ kV/cm and (b) top view for $\hat{E} = 9.63$ kV/cm.

drop [Fig. 5(b)]. The partial discharges only occur at specific locations on the boundary of the drop, depending on the orientation and shape of the drop. Similar to the gelatin drop, the discharges occur only at the sections which are oriented towards the electrodes. In addition, the arising cones or edges on the circumference of the drop, as observed on the right side of the drop, are more prone to partial discharges. The deformation of the drop and generation of cones or edges affects the field distribution around the drop by changing the curvature of the surface; hence, the electric field strength is locally increased. The exact prediction of the drop shape is rather complex because it depends on numerous influencing factors like local surface wetting or drop oscillations. Thus, the calculation of the partial discharge inception voltage for drops is more complex than originally presumed. The assumption of a capped spherical drop is no longer valid for a water drop generating partial discharges. The electric field strength at the inception of partial discharges is so high that the drop is always deformed. Due to the high electric field strength the deformation of the drops occurs even before the partial discharges. Nevertheless, the gelatin and water drops show a very similar behavior, and so gelatin drops can be used to investigate the partial discharge inception for nondeformed and stationary drops.

V. EXPERIMENTAL RESULTS AND DISCUSSION

The investigation of the partial discharge inception is performed with increasing complexity. First, single stationary gelatin drops are investigated. Afterwards, the inception field strength is determined for two neighboring gelatin drops. To investigate the impact of net charges, single water drops are used. Uncharged drops are investigated to act as a reference case to which results for drops containing a well-defined charge can be compared.

A. Single gelatin drops

The inception field strength of gelatin drops is of the same order of magnitude compared to the inception field strength of water reported in literature [18–20], which results from the similar behavior of gelatin and water inside the electric field. Figure 7 shows the inception field strength for single gelatin drops as a function of the drop volume for different substrates. The data show the mean value as well as the standard deviation of the mean value for the different volumes. Each data point is determined from at least 33 measurements in the case of silicone rubber and a minimum of 9 measurements for epoxy. As indicated by the data, an increasing volume leads to a reduction of the inception field strength. Furthermore, the inception field strength for a volume of $V = 100\ \mu$l is of the same order of magnitude for both epoxy and silicone. For large volumes ($V > 100\ \mu$l) the partial discharge inception field strength on epoxy is lower compared to silicone. The reason for the decrease of the inception field strength is the change of the contact angle. For a volume of $V = 100\ \mu$l both the contact angle for silicone rubber as well as for epoxy are similar ($\theta \approx 64.2^\circ$ and $\theta \approx 65.0^\circ$). The larger the volume of the drop, the larger is the difference of the contact angles. For a volume of $V = 300\ \mu$l the contact angles are $\theta \approx 71.5^\circ$ and $\theta \approx 61.4^\circ$ for silicone rubber and for epoxy, respectively. As already reported in literature, the contact angle influences the partial discharge inception [19] and is lower for epoxy compared to silicone due to its higher wettability. Hence, drops with lower contact angles are more prone to generate partial discharges.

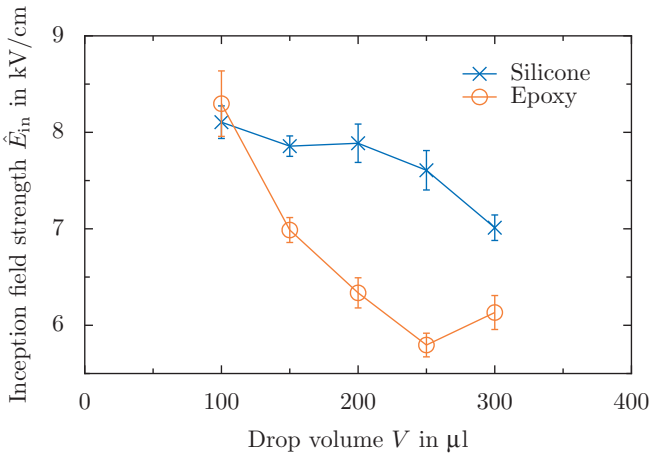

FIG. 7. Partial discharge inception field strength $\hat{E}_{in}$ ($f = 50$ Hz) for single gelatin drops depending on their volume on silicone rubber and epoxy. The error bars show the standard deviation of the mean value.

B. Interaction of two gelatin drops

In literature [19,35,36] several configurations with two or more drops have already been investigated, and results demonstrate that the inception field strength of partial discharges is lowered compared to single drops [19]. Nevertheless, the influence of the distance between the drops or the drop deformation was only examined superficially like in [37]. Detailed information about both influencing factors are still missing. In this study gelatin drops with a well-defined distance are used to investigate the interaction of two neighboring drops. The volume of the drops and the distance between the drops were varied to determine whether the drops interact with each other or not. In all the experiments the volume of both drops is identical.

Figure 8 shows an exemplary partial discharge pattern for two nearby gelatin drops. The image of the UV camera is superimposed onto a regular image of the drops. The location of the partial discharges is very similar compared to the single drop, but the strongest partial discharges are in between the drops, which is indicated by the higher intensity of the color. Hence, the neighboring drops enhance the electric field between the drops and, therefore, influence the electric field around each individual drop.

Figure 9 shows the partial discharge inception field strength as a function of the distance between the drops for different drop volumes. As expected, at large distances the inception field strength approaches the values corresponding to the single drop, shown in Fig. 7, because the distortion of the electrical field by the second drop reduces with distance and increases with volume. This is why the typical distance, at which the effect of the drop electrical interaction on the

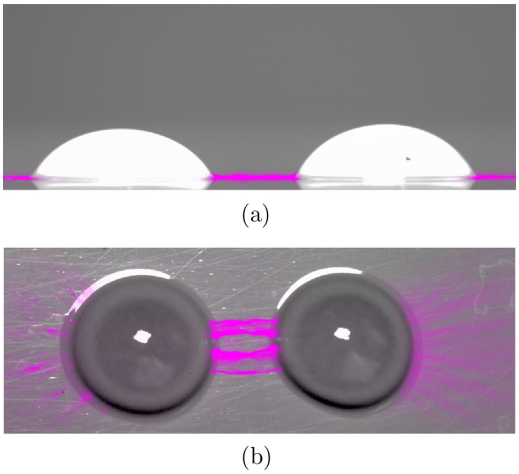

FIG. 8. Exemplary images of two gelatin drops: (a) $V \approx 60\ \mu$l and (b) $V \approx 150\ \mu$l with superimposed image of UV camera to visualize the partial discharges (colored in magenta) in (a) side view for $\hat{E} \approx 9.9$ kV/cm and (b) top view for $\hat{E} \approx 10.1$ kV/cm.

discharge is small, reduces with the drop size. Table I shows mean values of the inception field strength of the single drops.

Consequently, large sessile drops are much more prone to generate partial discharges compared to smaller drops. Note that the investigated gelatin drops do not move and therefore coalescence of the drops is impossible. In contrast, nearby water drops might coalesce due to their movement and oscillation. In case of a high-voltage insulator this behavior would lead to larger drops on the surface even if generally smaller drops (e.g., caused by rain or dew) are originally present on the surface. Hence, the aging of the substrate material due the partial discharges might be enhanced.

C. Influence of electric charge on inception field strength of water drops

Recently, the impact of net charge on the motion of drops was determined [29]. Both the net charge as well as the

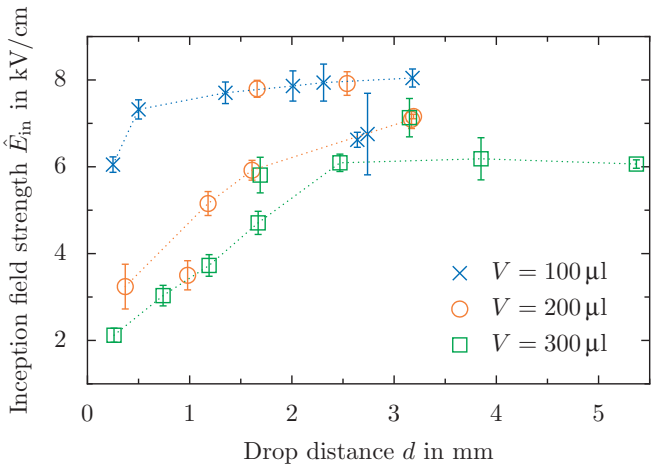

FIG. 9. Partial discharge inception field strength $\hat{E}_{in}$ of two gelatin drops depending on the distance for different volumes. The error bars show the standard deviation of the mean value.

TABLE I. Mean inception field strength for single gelatin drops, $\hat{E}_{in,single}$, compared to the inception field strength of a drop pair, $\hat{E}_{in,two}$, on silicone rubber depending on the volume. For $\hat{E}_{in,two}$ the converging limit value for large distances is taken into account. Single outliers are neglected.

Volume V (μl)	100	200	300
Single drop, $\hat{E}_{in,single}$ (kV/cm)	8.11	7.89	7.01
Drop pair $\hat{E}_{in,two}$ (kV/cm)	8.04	7.15	6.18

electric field strength determine the oscillation frequency of the drop. In addition, net charges on the drop influence the electric field around the drop and may also impact the partial discharge inception. The partial discharge inception for (assumed) uncharged drops was already investigated in the past and revealed a large influence of the wetting properties as well as the drop volume [18,20]. However, the impact of different oscillation modes was not investigated in detail. The oscillation of a sessile water drop significantly influences the shape of the drop and the contact angle, which might lead to an impact on the partial discharge inception. The principle motion of the drops in the first three resonance modes, including significant changes of the contact angle, are shown in Fig. 10. High-speed videos of the first three resonance motions can be found in the supplemental material of [29]. The oscillation of the drop is caused by the electric field and its resulting force on the drop. The oscillation modes correspond to the resonance frequencies f of the drop defined by [38,39]

$$f = \left[\frac{n(n-1)(n+2)\gamma}{12V\pi\rho}\right]^{1/2} \text{for } n \geqslant 2, \tag{2}$$

where ρ is the density of the liquid, V is the volume of the drop, and n is an integer corresponding to the mode number. The first resonance mode is defined by $n = 2$. Hence, the oscillation modes are mainly influenced by the drop volume and the frequency of the electric field.

To stimulate a specific resonance frequency of the drop with a specific volume, the frequency of the electric field was adapted according to Eq. (2). Hence, the drops were excited at a variable frequency depending on the drop volume and the intended resonance mode. Figure 11 shows the partial discharge inception voltage for uncharged water drops depending on the drop volume and different oscillation modes. The data points show the mean values and the error bars show the standard deviation of the mean value based on a minimum of four measurements. As shown in the figure, an increasing volume always leads to a decrease of the partial discharge inception field strength, independent of the resonance mode. Nevertheless, the impact of the volume decreases with increasing resonance frequency, and so with higher order modes. A possible reason might be the motion of the drop, which also depends on the resonance mode. A drop oscillating in mode 1 has a principle motion parallel to the substrate, which results in large changes of the contact angles. In contrast, the change of the contact angle decreases with higher resonance modes, because the principle motion is perpendicular to the substrate and the number of steady nodes on the surface of the drop is increased for resonance modes of higher order. A comparison

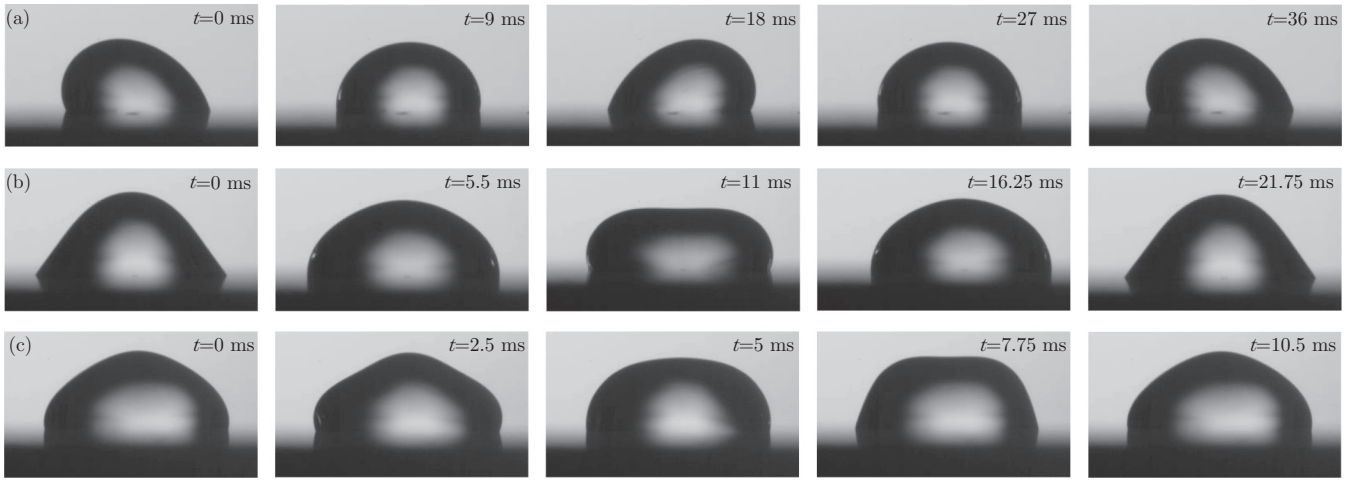

FIG. 10. One cycle of the first three modes for $n = 2, 3, 4$ of uncharged drops. (a) Example of mode 1 ($n = 2$) of a 20-μl drop at 27 Hz and $\hat{E} = 3.81$ kV/cm, (b) example of mode 2 ($n = 3$) of a 30-μl drop at 23 Hz and $\hat{E} = 4.67$ kV/cm and (c) example of mode 3 ($n = 4$) of a 60-μl drop at 48 Hz and $\hat{E} = 7.37$ kV/cm. Reprinted figure with permission from [29].

of the results with already existing measurements on silicone rubber shows that the partial discharge inception field strength is of the same order of magnitude [18–20,40]. The small deviation of the results might be caused by unwanted charges on the drop or different wetting properties of the used silicone rubber substrate.

Electric charges on drops can be unintentionally generated by, e.g., pipetting [41] or by charge transfer from the substrate to the drop [31]. Furthermore, technical applications might be influenced by charged drops, like high-voltage insulators, which are exposed to charged rain. To determine whether charges influence the partial discharge inception field strength or not, single water drops with different amounts of net charges are investigated under different conditions with respect to their resonance mode. The influence of the charge should be investigated independently from the motion of the drop to isolate the influence of electrical net charges. Due to the fact that the motion and oscillation are mainly determined by the electric charge as well as the applied field strength [29], the boundary conditions of the investigation have to be chosen accordingly. The motion of the drop as well as the oscillation frequency should be constant for the different amount of charges and electric field strengths to rule out any influence of the motion of the drop. As reported in [29], the motion of sessile drops oscillating in the first resonance mode is not affected by electric charges. The drop always oscillates with the same frequency as that of the applied voltage. Hence, the first resonance mode was chosen to investigate the influence of electric charges on the partial discharge inception field strength. Figure 12 shows the partial discharge inception field strength for single water drops on silicone rubber depending on the applied charge as well as the volume of the drops for resonance mode 1. The data points indicate the mean values, and the error bars show the standard deviation of the mean value based on a minimum of four measurements. Increasing the net charge on the drop decreases the inception

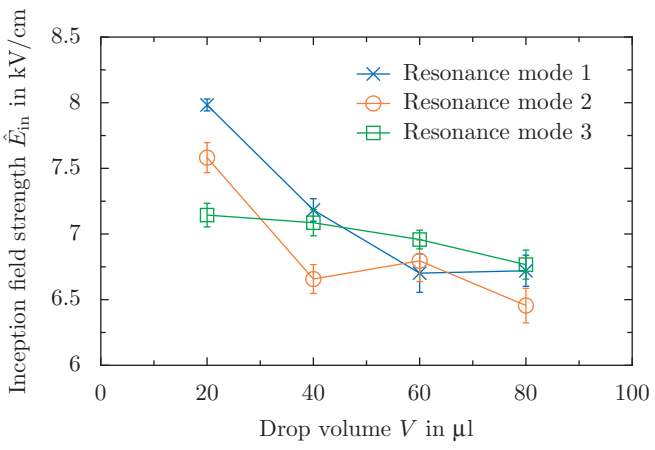

FIG. 11. Partial discharge inception field strength $\hat{E}_{in}$ of single uncharged water drops depending on the volume and resonance mode.

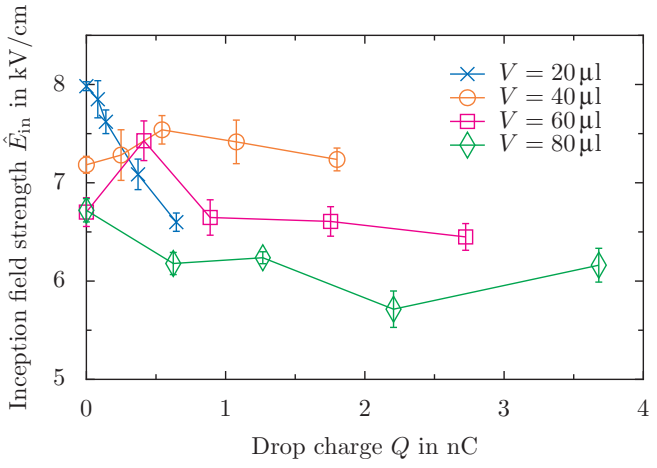

FIG. 12. Partial discharge inception field strength $\hat{E}_{in}$ of single water drops depending on the volume and electric charge for oscillation mode 1. The error bars show the standard deviation of the mean value.

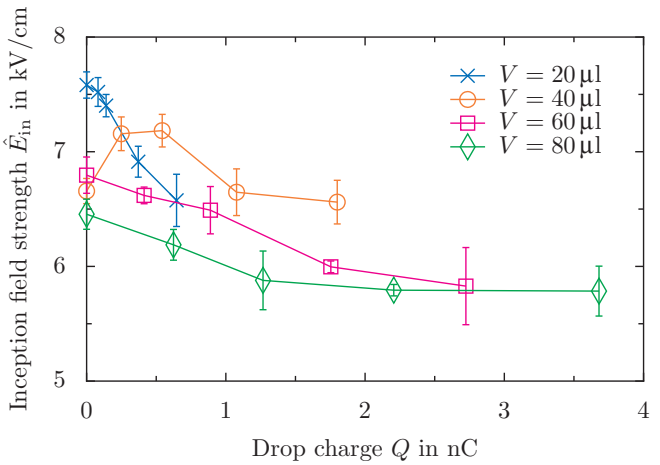

FIG. 13. Partial discharge inception field strength $\hat{E}_{\text{in}}$ of single water drops depending on the volume and electric charge for oscillation mode 2. The error bars show the standard deviation of the mean value.

field strength of partial discharges. The lower the volume of the drop, the stronger is the influence. The general influence of the volume that the inception field strength is lower for larger volumes is still observable. The applied charge on the drop leads to a distortion of the electric field around the drop resulting in strong field enhancements, which finally causes a decreased inception field strength of partial discharges.

A comparison of the different modes should reveal whether a change of the oscillation frequency impacts the inception of partial discharges or not. The oscillation frequency of the drop with a fixed volume is determined by both the electric charge and the electric field strength. A drop oscillating in resonance mode 2 or higher can oscillate with the same or with double the frequency of the applied voltage. Hence, the shape, including the contact angle, is affected by the drop frequency.

To determine the influence of the drop frequency both the electric charge as well as the electric field strength should be kept constant, because the generation of partial discharges strongly depends on the electric field strength. However, this is not possible, because an applied net charge reduces the inception field strength. This results in a different partial discharge pattern with respect to the number of impulses or the amount of apparent charge for both drops and a fixed electric field strength. Hence, the explicit interaction cannot, but the general influence of the changed mode can be determined. Figure 13 shows the partial discharge inception field strength for single water drops on silicone rubber depending on the drop charge for resonance mode 2. The data points indicate the mean values, and the error bars show the standard deviation of the mean value based on a minimum of four measurements. As already observed for resonance mode 1, an increasing amount of charge leads to a decrease of the partial discharge inception field strength.

Furthermore, an increasing volume also leads to a reduction of the inception of partial discharges. Comparing Figs. 12 and 13 reveals that the inception field strength in resonance mode 2 is generally lower than for mode 1, even if the oscillation in mode 1 causes larger changes of the contact angle. The behavior of drops oscillating in higher resonance modes is expected to be similar to resonance mode 2, because increasing the resonance frequency only increases the number of steady nodes on the surface of the drop. In addition, the uncharged drops oscillating in mode 3 were less affected compared to drops oscillating in mode 2. The principle direction of motion is still the same and the range of motion in terms of oscillation amplitude is smaller compared to lower modes.

VI. CONCLUSIONS

The partial discharge inception of sessile drops is influenced by several factors, like wetting properties, drop volume, and electric charge, as well as the oscillation of the drop. Gelatin drops can be used to generate stationary drops to investigate the partial discharge inception for fixed drops with nearly the same electrical properties as water drops. Using the stationary drops, the interaction of two neighboring drops was investigated, avoiding movement and coalescence of the drops. The smaller the distance between two drops, the lower is the inception field strength for partial discharges. Furthermore, the inception field strength of two neighboring drops strongly depends on the volume of the drops. The larger the drop volume, the stronger is the interaction of the drops. In addition, the influence of electric net charges on drops was investigated. Increasing the net charge leads to a decrease of the partial discharge inception field strength, independent of the drop volume. The experiments were performed in resonance mode 1 of the drops to ensure that the oscillation frequency of the drops was not affected by the charge and applied electric field. A comparison between the different oscillation modes revealed that increasing the resonance frequency leads to a decrease of the inception field strength of partial discharges. Consequently, the net charge of drops has a strong impact on the partial discharge inception, and charged drops are more prone to generate partial discharges, which may deteriorate the substrate. These results might be potentially useful for reliable modeling of the material aging (for example of high-voltage insulators) due to the partial discharges at the contact lines of the sessile drops.

ACKNOWLEDGMENTS

The authors would like to thank the Deutsche Forschungsgemeinschaft (DFG) for financial support of the project within the Collaborative Research Centre SFB-TRR 75, Project No. 84292822. Furthermore, the authors thank Florian Pabst for his support performing the dielectric spectroscopy.

[1] P. M. Vlahovska, Annu. Rev. Fluid Mech. **51**, 305 (2019).
[2] G. Taylor, Proc. R. Soc. A **280**, 383 (1964).
[3] Rayleigh, Philos. Mag. Ser. 5 **14**, 184 (1882).
[4] J. Plog, J.-M. Löwe, Y. Jiang, Y. Pan, and A. L. Yarin, Langmuir **35**, 11023 (2019).

[5] F. Mugele and J.-C. Baret, J. Phys.: Condens. Matter **17**, R705 (2005).
[6] P. Teng, D. Tian, H. Fu, and S. Wang, Mater. Chem. Front. **4**, 140 (2020).
[7] W. C. Nelson and C.-J. C. Kim, J. Adhes. Sci. Technol. **26**, 1747 (2012).
[8] J. Xie, J. Jiang, P. Davoodi, M. P. Srinivasan, and C.-H. Wang, Chem. Eng. Sci. **125**, 32 (2015).
[9] I. Hayati, A. I. Bailey, and T. F. Tadros, Nature **319**, 41 (1986).
[10] J. Xue, T. Wu, Y. Dai, and Y. Xia, Chem. Rev. **119**, 5298 (2019).
[11] J. Doshi and D. H. Reneker, J. Electrost. **35**, 151 (1995).
[12] C.-P. Chiu, T.-J. Chiang, J.-K. Chen, F.-C. Chang, F.-H. Ko, C.-W. Chu, S.-W. Kuo, and S.-K. Fan, J. Adhes. Sci. Technol. **26**, 1773 (2012).
[13] K. Mishra, C. Murade, B. Carreel, I. Roghair, J. M. Oh, G. Manukyan, D. van den Ende, and F. Mugele, Sci. Rep. **4**, 6378 (2014).
[14] N. C. Lima, A. Cavalli, K. Mishra, and F. Mugele, Opt. Express **24**, 4210 (2016).
[15] T. B. Jones, K. L. Wang, and D. J. Yao, Langmuir **20**, 2813 (2004).
[16] J. S. Hong, S. H. Ko, K. H. Kang, and I. S. Kang, Microfluid. Nanofluid. **5**, 263 (2008).
[17] *Springer Handbook of Experimental Fluid Mechanics*, edited by C. Tropea, A. Yarin, and J. F. Foss (Springer, Berlin, 2007).
[18] M. Nazemi and V. Hinrichsen, IEEE Trans. Dielectr. Electr. Insul. **22**, 1088 (2015).
[19] I. Lopes, S. H. Jayaram, and E. A. Cherney, IEEE Trans. Dielectr. Electr. Insul. **8**, 262 (2001).
[20] A. J. Phillips, D. J. Childs, and H. M. Schneider, IEEE Trans. Power Delivery **14**, 1081 (1999).
[21] B. Venkatesulu and M. J. Thomas, IEEE Trans. Dielectr. Electr. Insul. **18**, 418 (2011).
[22] Y. Hirano, T. Inohara, M. Toyoda, H. Murase, and M. Kosakada, IEEE Trans. Dielectr. Electr. Insul. **8**, 97 (2001).
[23] M. K. Moghadam, M. Taheri, S. Gharazi, M. Keramati, M. Bahrami, and N. Riahi, IEEE Trans. Dielectr. Electr. Insul. **23**, 1805 (2016).
[24] M. Bienia, M. Vallade, C. Quilliet, and F. Mugele, Europhys. Lett. **74**, 103 (2006).
[25] B. Shapiro, H. Moon, R. L. Garrell, and C.-J. C. Kim, J. Appl. Phys. **93**, 5794 (2003).
[26] M. Vallet, M. Vallade, and B. Berge, Eur. Phys. J. B **11**, 583 (1999).
[27] A. I. Drygiannakis, A. G. Papathanasiou, and A. G. Boudouvis, Langmuir **25**, 147 (2009).
[28] H. Wu, R. Dey, I. Siretanu, D. van den Ende, L. Shui, G. Zhou, and F. Mugele, Small **16**, e1905726 (2020).
[29] J.-M. Löwe, V. Hinrichsen, I. V. Roisman, and C. Tropea, Phys. Rev. E **101**, 023102 (2020).
[30] B. Sarang, P. Basappa, V. Lakdawala, and G. Shivaraj, in *2011 Electrical Insulation Conference (EIC) (Formerly EIC/EME)* (IEEE, USA, 2011), pp. 377–381.
[31] J.-M. Löwe, M. Secklehner, and V. Hinrichsen, in *INSUCON 2017: Proceedings of the 13th INSUCON International Electrical Insulation Conference* (IEEE, Piscataway, NJ, 2017), pp. 1–7.
[32] M. Brandenbourger and S. Dorbolo, Can. J. Phys. **92**, 1203 (2014).
[33] A. Angulo-Sherman and H. Mercado-Uribe, Chem. Phys. Lett. **503**, 327 (2011).
[34] *Electromagnetic Aquametry: Electromagnetic Wave Interaction with Water and Moist Substances*, edited by K. Kupfer (Springer-Verlag, Berlin, 2005).
[35] G. Xie, F. He, X. Liu, L. Si, and D. Guo, Sci. Rep. **6**, 25002 (2016).
[36] S. M. Rowland and F. C. Lin, J. Phys. D: Appl. Phys. **39**, 3067 (2006).
[37] M. H. Nazemi, Ph.D. thesis, Technische Universität Darmstadt, Darmstadt, 2016.
[38] T. Schütte and S. Hornfeldt, in *IEEE International Symposium on Electrical Insulation* (IEEE, New York, 1990), pp. 202–207.
[39] H. Lamb, *Hydrodynamics* (Cambridge University Press, Cambridge, UK, 1895).
[40] M. H. Nazemi and V. Hinrichsen, IEEE Trans. Dielectr. Electr. Insul. **20**, 443 (2013).
[41] D. Choi, H. Lee, D. J. Im, I. S. Kang, G. Lim, D. S. Kim, and K. H. Kang, Sci. Rep. **3**, 2037 (2013).